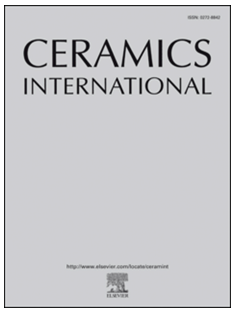

Ultrasensitive NO_2 gas sensing performance of two dimensional ZnO nanomaterials: Nanosheets and nanoplates

Lai Van Duy, To Thi Nguyet, Chu Manh Hung, Dang Thi Thanh Le, Nguyen Van Duy, Nguyen Duc Hoa, Franco Biasioli, Matteo Tonezzer, Corrado Di Natale

PII: S0272-8842(21)02069-1

DOI: https://doi.org/10.1016/j.ceramint.2021.07.042

Reference: CERI 29347

To appear in: *Ceramics International*

Received Date: 27 March 2021

Revised Date: 20 May 2021

Accepted Date: 4 July 2021

Please cite this article as: L. Van Duy, T.T. Nguyet, C.M. Hung, D.T. Thanh Le, N. Van Duy, N.D. Hoa, F. Biasioli, M. Tonezzer, C. Di Natale, Ultrasensitive NO_2 gas sensing performance of two dimensional ZnO nanomaterials: Nanosheets and nanoplates, *Ceramics International* (2021), doi: https://doi.org/10.1016/j.ceramint.2021.07.042.

Ultrasensitive NO_2 gas sensing performance of two dimensional ZnO nanomaterials: nanosheets and nanoplates

Lai Van Duy[1], To Thi Nguyet[1], Chu Manh Hung[1], Dang Thi Thanh Le[1], Nguyen Van Duy[1*], Nguyen Duc Hoa[1*], Franco Biasioli[2], Matteo Tonezzer[2,3,4], Corrado Di Natale[5]

[1] International Training Institute for Materials Science (ITIMS), Hanoi University of Science and Technology (HUST), No 1, Dai Co Viet Street, Hanoi, Vietnam

[2] Department of Food Quality and Nutrition, Research and Innovation Centre, Fondazione Edmund Mach, 38010, San Michele all' Adige, TN, Italy

[3] IMEM-CNR, Sede di Trento-FBK, Via alla Cascata 56/C, 38123 Povo-Trento, Italy

[4] Center Agriculture Food Environment, University of Trento/Fondazione Edmund Mach, via E. Mach 1, 38010 San Michele all'Adige, Italy

[5] Department of Electronic Engineering, University of Rome Tor Vergata, 00133 Rome, Italy

* Corresponding authors: ndhoa@itims.edu.vn, nguyenvanduy@itims.edu.vn

Abstract

Highly sensitive NO_2 gas sensors with low detection limit are vital for practical application in air pollution monitoring. Here, the NO_2 gas sensing performance of porous ZnO nanosheets and nanoplates were investigated, with different shape and thickness. It was found that ultra-thin ZnO nanoplates had a higher sensitivity than coral-like ZnO nanosheets. The results were attributed to the high specific surface and very small thickness of the ultrathin nanoplates. The nanoplates have indeed a thickness of 15 nm compared to that of the nanosheets which is 100 nm, and a BET surface area of 75 m^2/g, while that of the nanosheets is 6 m^2/g. The chemosensor based on ultra-thin ZnO nanoplates shows a response (calculated as the ratio between the resistance of the sensor in the presence of the gas and in its absence) of 76 to 0.5 ppm of NO_2 at 200°C, with a theoretical detection limit of 3 parts per trillion and a selectivity higher than 760 towards acetone, ethanol, isopropyl alcohol, triethylamine, SO_2 and CO. The specific surface and the small thickness of the ultra-thin nanoplates contribute to its highly improved sensing performance, making it ideal for NO_2 gas sensing.

Keywords: NO_2; gas sensor; ZnO; nanoplates; nanosheets

1. Introduction

According to the World Health Organization (WHO), more than 90% of the world's population lives in areas that exceed air pollution limits, nearly 98% of cities in low-income countries do not meet air quality standards, and about 3 million people lose their lives each year due to pollution-related disorders [1]. One of the most toxic gases present in the atmosphere is nitrogen dioxide (NO_2), a reddish-brown gas with a characteristic sharp odor [2]. There is a lot of interest in monitoring this gas and reducing its concentration, due to its harmful effects on human health and the environment [3]. Nitrogen dioxide is mainly produced from the industrial exhaust gas, power plants, petrochemical plants, vehicles and laboratories [4]. It can produce photochemical pollution and acid rain, as well as irritation to the eyes and lungs, respiratory diseases, weakening of the immune system and even death [3,5].

According to the WHO and the European Commission for Air Quality Standards, the NO_2 hourly mean value may not exceed 0.1 parts per million (ppm) more than 18 times in a year, while the NO_2 annual mean value may not exceed 0.02 ppm [6]. In the environment, the NO_2 concentration is on the order of ppb, making it difficult to detect [3]. For these reasons, different types of devices have been studied recently, trying to obtain NO_2 sensors that are very sensitive, reliable, and selective. NO_2 chemical gas sensors based on semiconductor metal oxides (SMOs) are very promising due to their advantages such as low manufacturing cost, simple operation, low power consumption, high sensitivity and stability, and good compatibility with silicon technology [3,7–9].

Among the various sensing technologies, solid state chemoresistors are among the most used for NO_2 detection, and among the most used materials several SMOs are found: SnO_2, ZnO, In_2O_3, V_2O_5, WO_3 and TiO_2 [10–12]. Recently, heterostructures based on combinations of these semiconductors or on the surface decoration with metallic nanoparticles such as Pt, Au and Ag have been deeply studied [13]. Zinc oxide is one of the most studied SMOs for its properties, and it has been used widely to realize different types of devices, namely gas sensors [14,15],

electrochemical sensors and biosensors [16,17] but also supercapacitors [15] and environmental tools for pollution degradation [16].

Furthermore, ZnO proved to have some natural selectivity towards NO_2 [17–19]. For instance, Wang et al. [20] incorporated ZnO nanowires and black phosphorus nanosheets for the detection of NO_2 gas with enhanced response value. Zhou et al. [21] used nanowire-network sensor for the detection of NO_2 gas under UV illumination, where they studied the effect of carrier gas on the sensing performance. Such sensors could detect NO_2 at ppb level at room temperature, but the sensors required long response and recovery time. Recently, improvements in nanotechnology allow for better control of ZnO nanostructures in terms of crystal structure, size and dimensionality, porosity and microstructure on the mesoscale [22–24]. The geometry and size of the ZnO nanostructures are particularly important in the case of gas sensors due to the great influence that morphology has on gas detection performance. Wang et al. developed a sensor based on ZnO nanospheres that exhibits a response of 29.4 to 5 ppm of NO_2 at room temperature when illuminated with ultraviolet (UV) light [17]. Due to their larger surface area and the small diameter of the nanoparticles that compose them, the nanospheres showed a better response than nanorods and nanoflowers. The response of all ZnO nanostructures was very low for all other gases tested (NO, CO, NH_3, C_6H_6, H_2, ethanol and acetone), indicating excellent shape-independent selectivity. Kusumam et al. have shown that very thin nanosheets (thickness of 30 nm) give a much greater response than nanoparticles with a diameter of 100 nm: a response of 260% to 5 ppm of NO_2 and a sensitivity of 21%/ppm [23].

In this work, porous coral-like nanosheets and ultra-thin ZnO nanoplates were grown by hydrothermal technique followed by thermal annealing. The sensor based on the ultra-thin nanoplates exhibits superior NO_2 sensing performance compared to the coral-like nanosheets counterpart. It can detect very low NO_2 concentrations with a detection limit of 3 parts per trillion at the optimal working temperature of 200°C. The response of the ultra-thin ZnO nanoplates was 76 to 0.5 ppm NO_2, twice that of the porous coral-like ZnO nanosheets. The

selectivity of the sensor with respect to interferents (acetone, ethanol, isopropyl alcohol, triethylamine, SO_2 and CO) is higher than 760. This excellent performance, combined with the advantages of chemoresistors based on metal oxide nanostructures (reduced size and cost, simplicity of fabrication and measurement), make the ultra-thin ZnO nanoplates an ideal material for NO_2 sensors.

2. Experimental

The chemicals used in this work ($ZnSO_4 \cdot 7H_2O$, urea (CH_4N_2O) and $Zn(NO_3)_2 \cdot 6H_2O$) were bought from Sigma-Aldrich. All reagents were analytic grade and used as received without further purification. Both porous ZnO nanostructures were synthesized by hydrothermal method (Fig. 1), using deionized water as solvent.

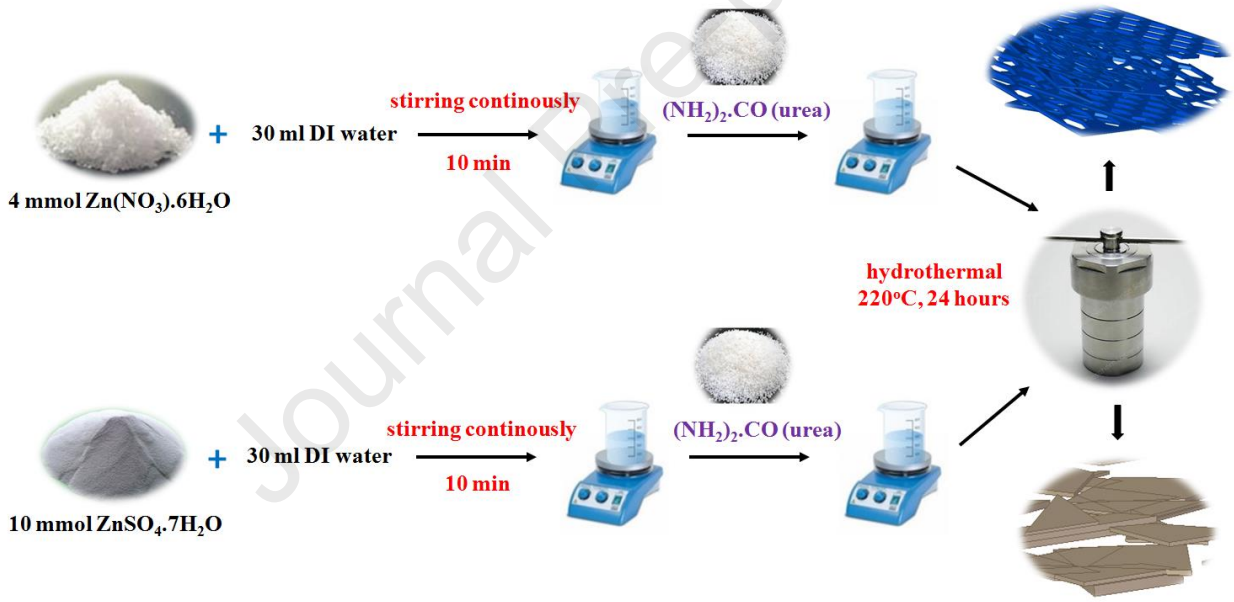

Figure 1. Hydrothermal synthesis procedure of ZnO nanosheets and nanoplates.

In a typical process to grow ZnO nanosheets, zinc nitrate hexahydrate [$Zn(NO_3)_2 \cdot 6H_2O$] (4 mmol) was dissolved in 30 mL deionized water under continuously stirring for 15 min. Then 20 ml urea (CH_4N_2O) solution (8 mmol) was added with further stirring for 15 min to obtain pH 5. The resulting solution was transferred into a 100 ml Teflon-lined stainless-steel autoclave, where it was maintained at 220°C for 24 h for the hydrothermal growth. After being naturally cooled to

room temperature, the precipitate on the bottom was centrifuged, washed several times with deionized water, then with ethanol solution, and finally collected by centrifugation at 4000 rpm. The obtained white powder was dried in an oven at 60°C for 24 h, and then calcined at 600°C [27].

The ultra-thin ZnO nanoplates were grown following a very similar procedure (Fig. 1). Zinc sulfate heptahydrate [$ZnSO_4 \cdot 7H_2O$] (10 mmol) was dissolved in 30 mL deionized water. After continuously stirring for 15 min, 20 mL urea solution (20 mmol) was added with further stirring for 15 min to adjust the pH to 5. The resulting solution was then transferred into a Teflon-lined stainless-steel autoclave and the hydrothermal process was maintained for 24 h at 220°C. The washing and collecting process of the nanomaterial was the same as that for the porous ZnO nanosheets [28].

The synthesized materials were characterized by field-emission scanning electron microscopy (SEM, JEOL 7600F), powder x-ray diffraction (XRD, Advance D8, Bruker), and high-resolution transmission electron microscopy (HRTEM, JEOL 2100F). The specific surface area of the nanomaterials was determined using Brunauer–Emmett–Teller nitrogen adsorption/desorption isotherms (Micromeritics Gemini VII). The sensing properties of the synthesized coral-like ZnO nanosheets and ultra-thin ZnO nanoplates were then characterized by using a laboratory-made system. Prior to the gas sensing measurements, the sensor was preheated at 600°C for 2 h in order to improve the adhesion between Pt electrodes and materials and to stabilize the sensor output. This also eliminate the effect of heat treatment condition on the gas sensing performance of the fabricated sensors for comparison. Sensor resistance was measured continuously using a source meter (Keithley 2602) while the chamber was flowed with different concentrations of gas, intersperse with dry air. Schematic diagram of the gas sensing measurement system was reported in ref. [29]. The sensing measurement setup consists of a heater, a temperature controller, gas inlet and outlet valves, and probes connecting the sensor to Keithley 2602 source meter (Fig. S1, Supplementary). Target gases (NO_2, SO_2, and VOCs) of different concentrations were prepared

by mixing standard gases with dry air as reference and dilution using a series of mass flow controllers. Details about the calculation of target gas concentration can be found in our recent publication [30]. The response (S) was calculated as the ratio R_a/R_g (for reducing gases) or R_g/R_a (for oxidizing gases), where R_a and R_g were the resistances of the sensor in dry air and tested gas, respectively. The response and recovery times (τ_{resp}, τ_{recov}) were defined as the time taken by the sensor to reach 90% of its saturated response after exposure to NO_2 and air, respectively [24].

3. Results and discussion

Typical SEM images of coral-like ZnO nanosheets and ultra-thin ZnO nanoplates are shown in Figure 2.(A, B) and Figure 2.(C, D), respectively. Both materials show a high homogeneity, with two-dimensional nanostructures about one micron wide, randomly oriented. The nanosheets in Fig. 2(A,B) have very large size, with an average thickness of about 100 nm and show a marked porosity (pores of about 90 nm in diameter). The nanoplates in Fig. 2(C, D) look smooth and have an average thickness of 15 nm. Herein, homogenous coral-like ZnO nanosheets and ultra-thin ZnO nanoplates were obtained without using any surfactant, thus reducing the usage of chemicals.

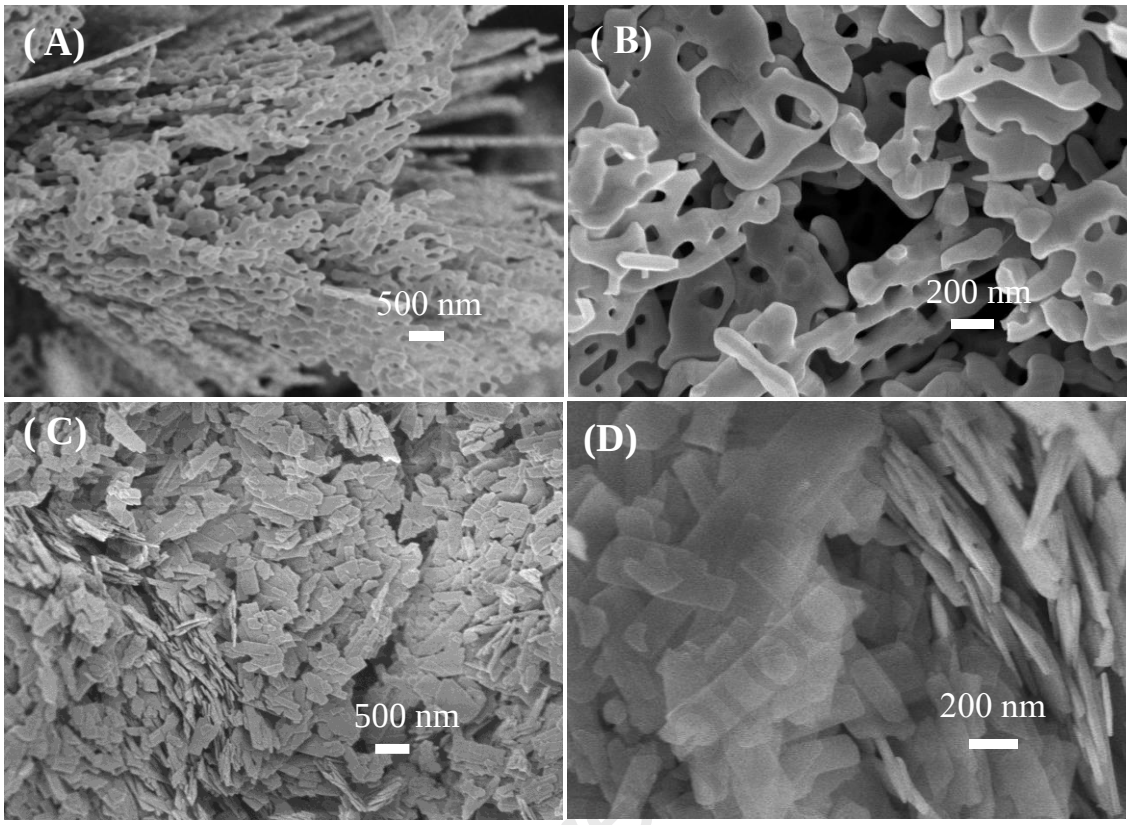

Figure 2. SEM images of the synthesized ZnO nanostructures: (A, B) coral-like nanosheets and (C,D) ultra-thin nanoplates.

The mechanism of formation of coral-like ZnO nanosheets and ultra-thin ZnO nanoplates can be explained as follows: zinc sulphate heptahydrate, and zinc nitrate hexahydrate are used as precursor of Zn^{2+}, while urea is used as a means to control the pH of the solutions. During the hydrothermal process, urea is easily broken down into NH_3 and HNCO [25], and CH_4N_2O decomposes into NH_4OH and HNCO [26]. Therefore, the $(OH)^-$ group reacts with Zn^{2+} ions to form $Zn(OH)_2$ flakes. The morphology and thickness of the ZnO nanostructures were attributed to the use of precursor salts.

The lattice structure of the ZnO nanosheets and nanoplates was analyzed by means of XRD, the patterns of which are shown in the upper panel of Fig. 3A. The experimental patterns for coral-like nanosheets (in red) and ultra-thin nanoplates (in blue) show the same peaks, which match well with those of the wurtzite crystal structure (JCPDS card No. 36-1451), shown in the lower panel. The intense and sharp peaks indicate a good crystallinity of the nanostructures composing both sensors. No peaks due to other phases or amorphous contributions are visible, confirming

the good crystallinity and single phase of the nanomaterials [31]. The crystallite size was calculated using Scherrer formula, resulting in 21.2 nm for coral-like nanosheets and 19.6 nm for ultra-thin nanoplates. The specific surface of the coral-like ZnO nanosheets and ultrathin nanoplates was tested with nitrogen adsorption/desorption isotherm measurements, the results of which are shown in Fig. 3B. Despite their marked porosity, coral-like nanosheets have a BET surface area of 6 m^2/g, while ultra-thin nanoplates have a much larger BET surface area of 75 m^2/g. The large surface area, together with the tiny thickness of the nanoplates are two important factors why the nanoplates are expected to have better sensing performance than the coral-like nanosheets [32].

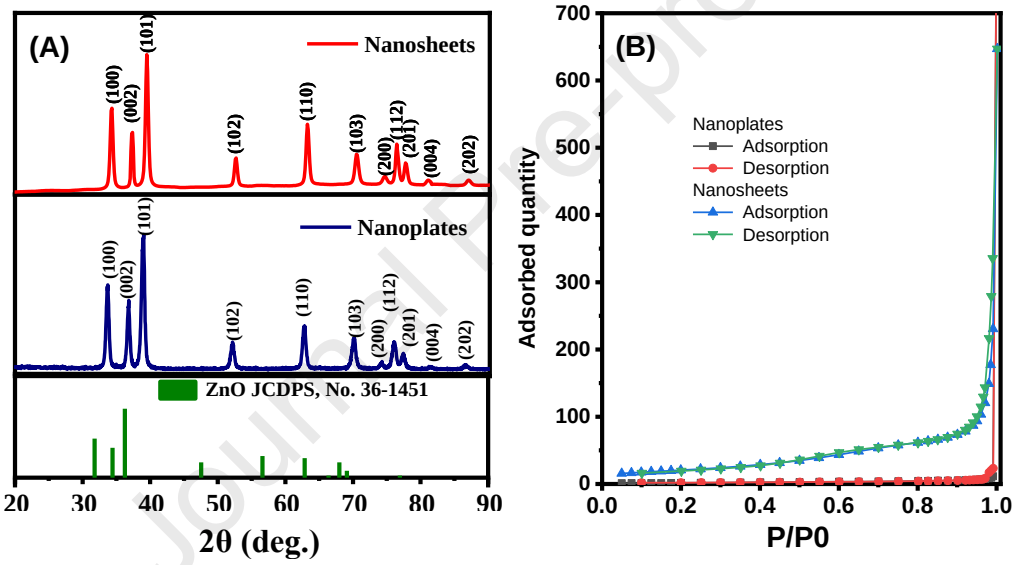

Figure 3. (A) XRD patterns, and (B) Nitrogen adsorption/desorption of the synthesized ZnO nanosheets and ZnO nanoplates.

Typical TEM images of the coral-like ZnO nanosheets and ultra-thin ZnO nanoplates are shown in Figure 4. Fig. 4A and C show low magnification TEM images confirming the morphologies of porous nanosheets, and ultra-thin nanoplates, respectively. The size of ZnO nanosheets is very large of micrometers with many nanopores. The nanoplate are smaller with a size of about 100 nm. The HRTEM images in Fig. 4B and D clearly show the lattice fringes confirming the good crystallinity of both nanostructures. The interplanar spacing was found to be 0.25 and 0.50 nm in coral-like nanosheets and ultrathin nanoplates, respectively. The interspacing between two

adjacent planes 0.25 and 0.50 nm are in good agreement with the expected values for (101), and (001) of the hexagonal ZnO.

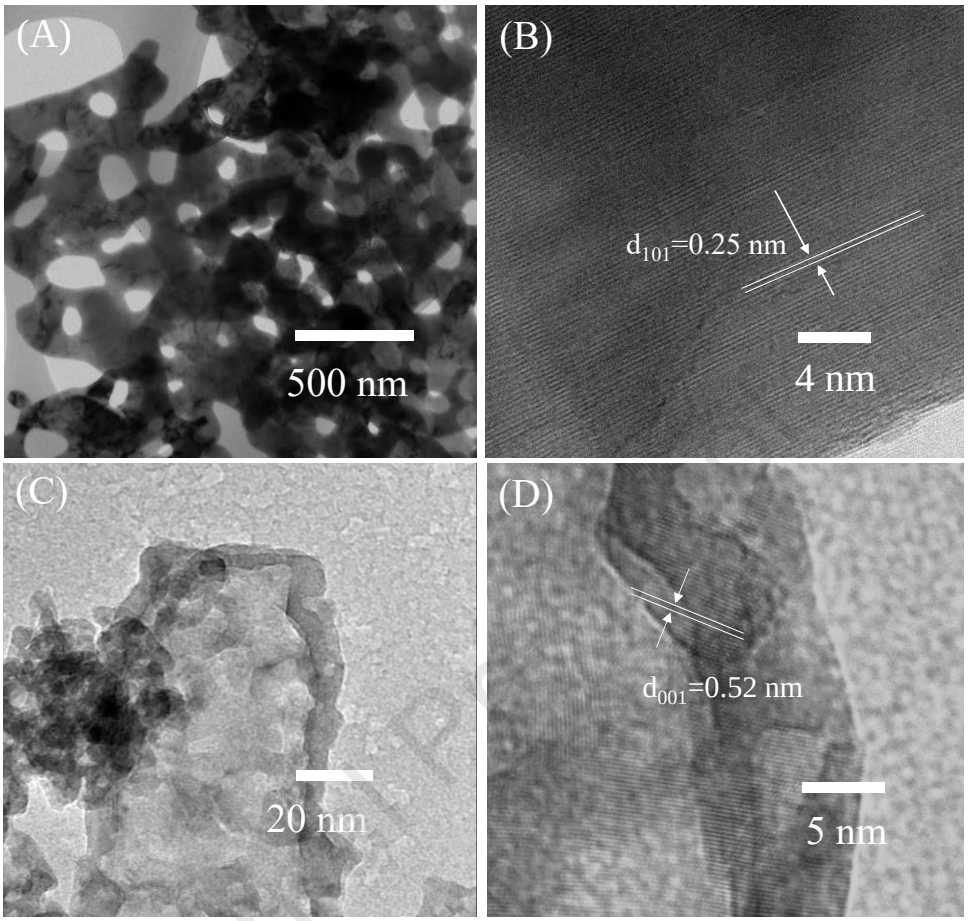

Figure 4. TEM images of (A-B) the coral-like ZnO nanosheet and (C-D) ultrathin porous ZnO nanoplates.

The *I–V* curves of the sensors based on the two individual nanomaterials in air are shown in figures 5A and C. A voltage range from −5 V to +5 V was applied to the sensors. Both sensors of showed linear *I–V* characteristics, demonstrating good ohmic contact between the ZnO nanostructures and the electrodes. Figure 5B and D show the resistance of the coral-like ZnO nanosheets and ultra-thin ZnO nanoplates in air at different working temperatures. The coral-like ZnO nanosheet sensor showed the maximum resistance at 300^{o}C, whereas the ZnO nanoplate device exhibited the maximum resistance at 250^{o}C. The results are very interesting, because it is agreed that the resistance of a semiconductor decreases with an increase of temperature. However, here, the resistance of sensors increased with an increase of temperature from 200 to 250 for the ZnO nanoplate sensor and to 300 for the ZnO nanosheet sensor. Such behaviors

could be explained by the competition between the decrease of resistance due to the thermal excitation of electron from valent band to conduction band, and the increase of resistance caused by the surface adsorption of oxygen species. With temperature increasement from 200 to 250, and 300ºC the oxygen adsorption dominates the change in resistance, thus the sensor resistance increased, and archived the maximum values. To clarify this point, we tested the *I-V* curves of the nanosheet sensor in N_2 at high temperatures, and the data are shown in Fig. S2 (Supplementary). The sensor showed linear *I-V* curves at all measured temperatures (Fig. S2A, Supplementary). In addition, the sensor resistance decreases with an increase of temperature from 150 to 350ºC (Fig. S2B, Supplementary). No peak of resistance was detected at 300ºC as obverted when testing in air. Such results confirm that the oxygen adsorption play an important role in determination the change in based resistance of sensor with temperature.

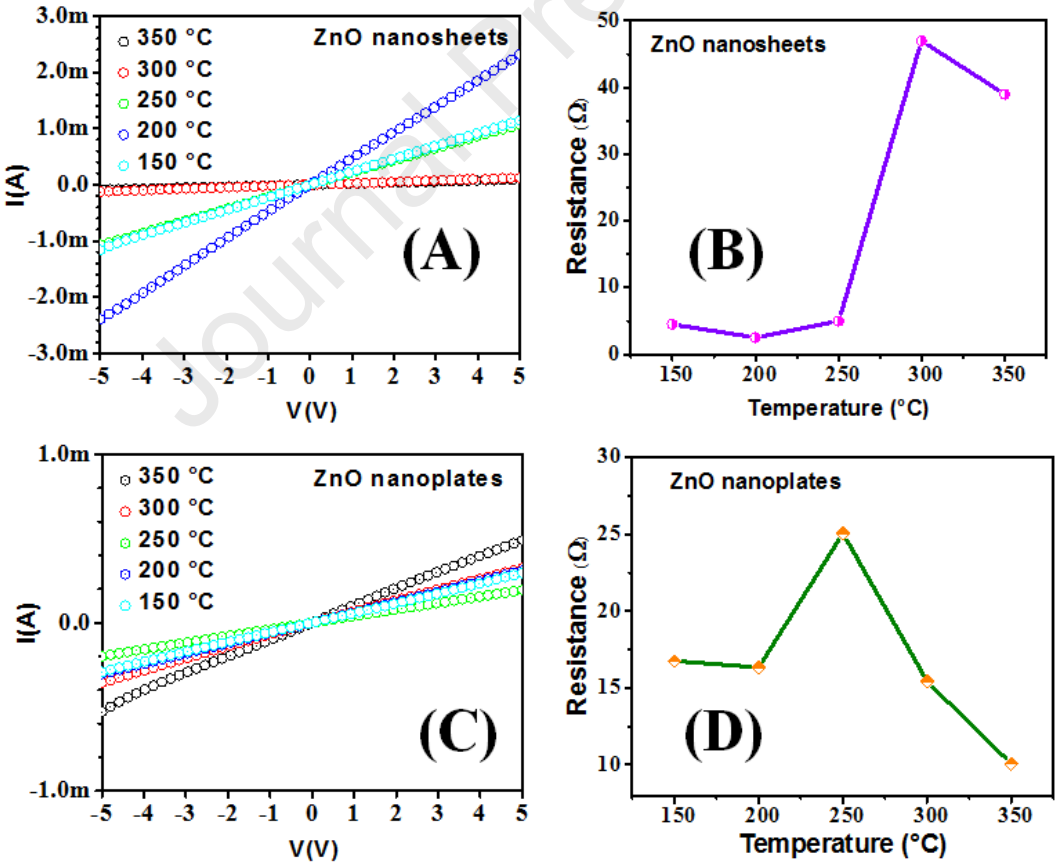

Figure 5. *I–V* curve of the ZnO nanosheets (A) and ZnO nanoplates (C) sensor measured in air at 150 - 350˚C; calculated resistance at different working temperatures for (B) ZnO nanosheets and (D) ultra-thin nanoplates.

Figures 6A and 7A show the dynamic resistance of the coral-like ZnO nanosheets and ultra-thin ZnO nanoplates when different concentrations of NO_2 were injected at different temperatures. The ZnO nanostructures were tested with 10, 5, 2.5, 1, and 0.5 ppm of NO_2, in a temperature range of 150-350°C. The sensor resistance rapidly increases when exposed to NO_2 gas, and returns to its base value when NO_2 flow is stopped and replaced with air. This effect is expected for an n-type semiconductor reacting to an oxidizing gas, which withdraws electrons from the nanostructures. The response values calculated from Fig. 6A and 7A for coral-like ZnO nanosheets and ultra-thin ZnO nanoplates, are shown in Fig. 6B and 7B, respectively. While the response of nanosheets is linear throughout the concentration range, that of nanoplates tends to saturate beyond 2 ppm. For both nanostructures, the optimal temperature (at which the response is maximum) is 200°C. The response of ultra-thin nanoplates is significantly higher than that of coral-like nanosheets, especially at lower concentrations: at 200°C the response of nanoplates to 1 ppm of NO_2 is 156, which is more than 2 times that of nanosheets. Fig. 6C and fig. 7C show the response and recovery time of the coral-like ZnO nanosheets and the ultra-thin ZnO nanoplates sensors, calculated at 200°C to different concentrations of NO_2. Response times are in the order of tens of seconds, while recovery times are in the order of minutes. The ultra-thin nanoplates respond and recover faster than the coral-like nanosheets, probably due to their thinness and larger surface.

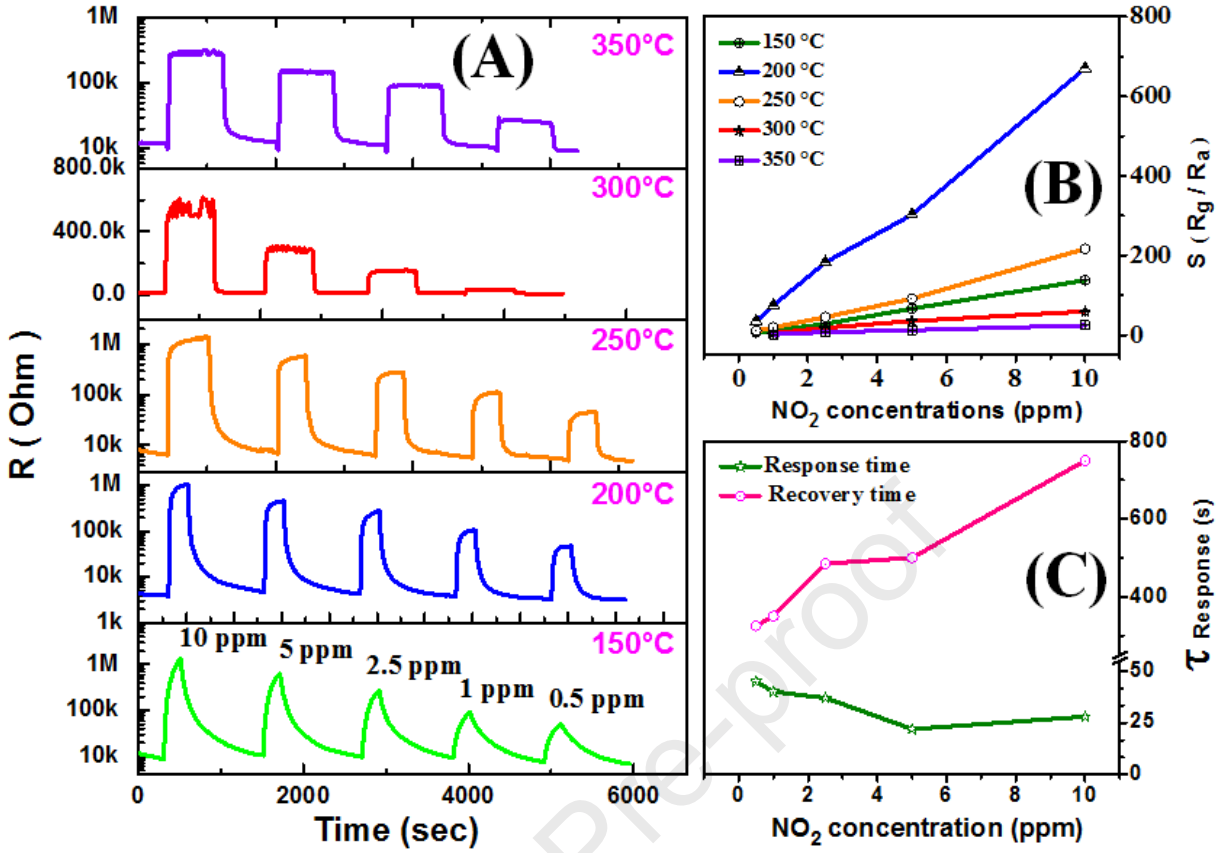

Figure 6. NO_2 sensing performance of the coral-like ZnO nanosheets: (A) dynamic resistance upon exposure to different concentrations of NO_2 measured at different temperatures; (B) sensor response as a function of NO_2 concentration; (C) response and recovery time as a function of the NO_2 concentration.

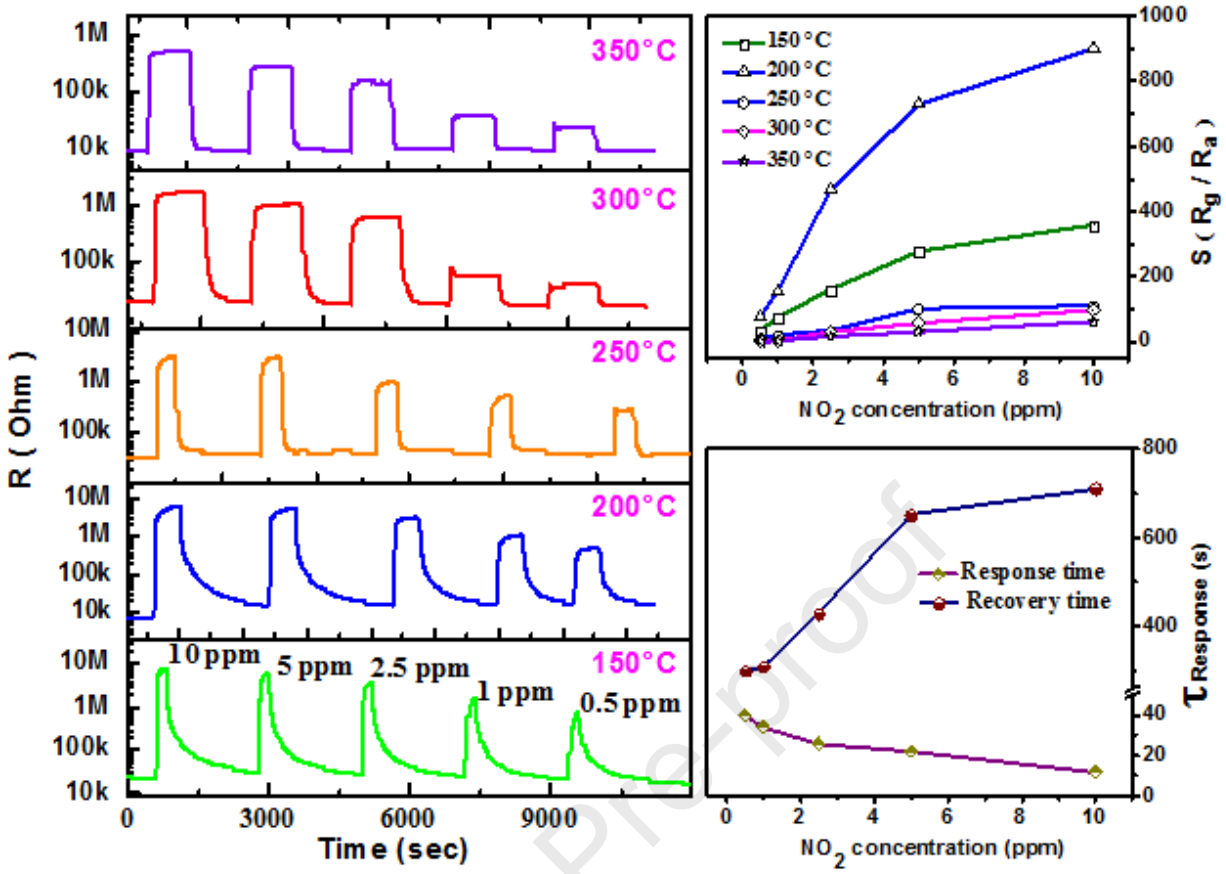

Figure 7. NO_2 sensing performance of the porous ZnO nanoplates: (A) dynamic resistance upon exposure to different concentrations of NO_2 measured at different temperatures; (B) sensor response as a function of NO_2 concentration; (C) response and recovery time as a function of the NO_2 concentration.

The NO_2 detection limit (DL) of the sensors based on the coral-like ZnO nanosheets and ultra-thin ZnO nanoplates, was calculated at their optimal operating temperature of 200°C. Although the lowest gas concentration investigated in this study is of 0.5 ppm, the sensor theoretical detection limit can be determined by the formula: $DL=3\cdot SD_{noise}/Sensitivity$, which is the IUPAC definition with k = 3 [29]. In the formula SD_{noise} is the standard deviation of the sensor noise measured in air, while *Sensitivity* is the derivative of its response as a function of NO_2 concentration, calculated at the minimum concentration. Details on the calculation method of detection limit can be found elsewhere [30]. At 200°C the ultra-thin ZnO nanoplates sensor has a detection limit of 3 ppt, which is lower than that of the coral-like ZnO nanosheets sensor, which

is 25 ppt.

Table 1. shows NO_2 sensing performance of ZnO nanostructures in scientific literature. As can be seen, the response of ultra-thin nanoplates is very high, while the detection limit is orders of magnitude lower than the others reported. Such low detection limit is advantageous in practical application in monitoring of ultralow concentration of NO_2 gas in air pollution monitoring.

Table 1. NO_2 sensing performance of ZnO nanostructures in scientific literature.

Morphology	**Size (nm)**	**NO_2 concentration (ppm)**	**Temperature (°C)**	**Response (R/R_0)**	**Detection limit***	**Ref**
Nanorods	Ø 150-200	1	300°C	1.8 (1 ppm)	<1 ppm	[34] (2006)
Nanorods	Ø 30	0.2-5	250°C	200 (5 ppm)	0.2 ppm	[35] (2009)
Nanotubes	Ø 200	1-20	150°C	1.31 (1 ppm)	1 ppm	[36] (2009)
Nanorods	Ø 60	0.1-1	200°C	1.3 (100 ppb)	100 ppb	[24] (2013)
Nanopetals	Thickness 70	20	RT	119 (20 ppm)	20 ppm	[37] (2015)
Nanorods	Ø 260	1-100	200°C	1.41 (1 ppm)	1 ppm	[36] (2017)
Nanowires	Ø 80-90	1-30	250°C	1.3 (1 ppm)	1 ppm	[38] (2018)
Rose-like hierarchical structures	Flowers: Ø 200 Sheet: thickness 10	5-80	300°C	49 (10 ppm)	5 ppm	[39] (2018)
Nanorods	Ø 50-300	0.1-5	25°C + UV	1.6 (0.5 ppm)	100 ppb	[40] (2021)
Flowers	Sheet thickness: 30			2.0 (0.5 ppm)		
Sphere	NPs Ø 20-30			2.2 (0.5 ppm)		
Nanoplates	Thickness 15	0.5-10	200°C	156 (1 ppm)	3 ppt	This work

* When the detection limit was not calculated, the lowest measured concentration was reported.

To evaluate the short–term stability of the coral-like ZnO nanosheets and ultra-thin ZnO nanoplates sensors, we investigated 8 recovery-response cycles to 1 ppm NO_2 at 200°C. The results are shown in Fig. 9 and indicate that both sensors are very stable and repeatable.

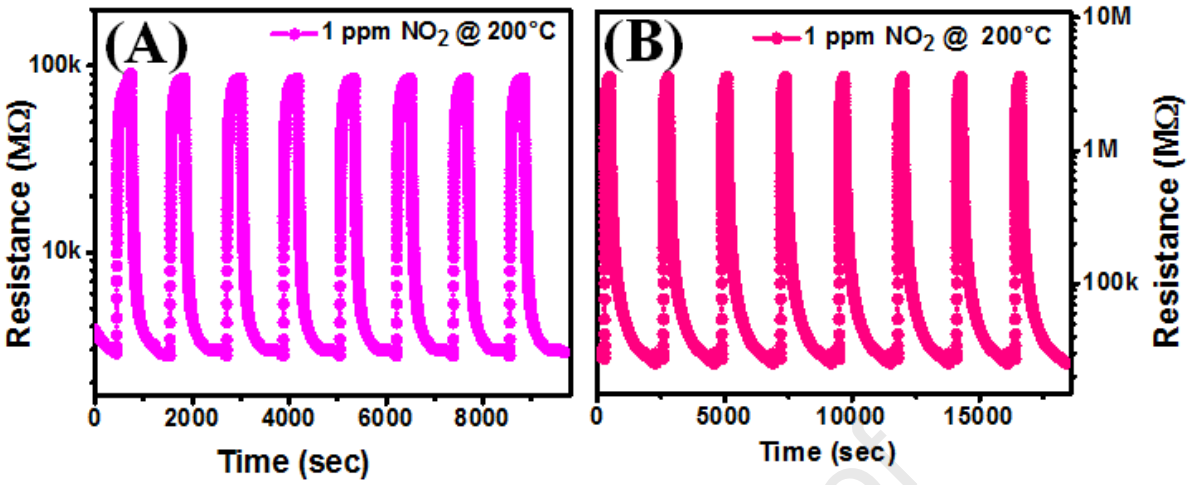

Figure 9. Short–term stability of (A) ZnO nanosheets and (B) ZnO nanoplates sensor to NO_2.

Selectivity is considered an important parameter for practical applications. The ultra-thin ZnO sensor was tested to various concentrations of interfering gases such as 0.5 ppm NO_2, 500 ppm acetone, 500 ppm ethanol, 500 ppm isopropyl alcohol, 500 ppm triethylamine, 5 ppm SO_2, and 200 ppm CO at a working temperature of 200°C, as shown in Figure 10. The sensor exhibits the highest response to NO_2, followed by CO, SO_2, acetone, triethylamine, isopropyl alcohol, and ethanol. The sensor response to NO_2 is much higher than that to all the interfering gases tested, although the NO_2 concentration was much lower than those of the other gases (in most cases by a thousand times). Note that the sensor is highly selective to even oxidant SO_2 gas, where the response value is about 1.58 for 5 ppm SO_2. This suggests the potential application of the ultra-thin ZnO nanoplates sensor for selective detection of NO_2 in air quality monitoring.

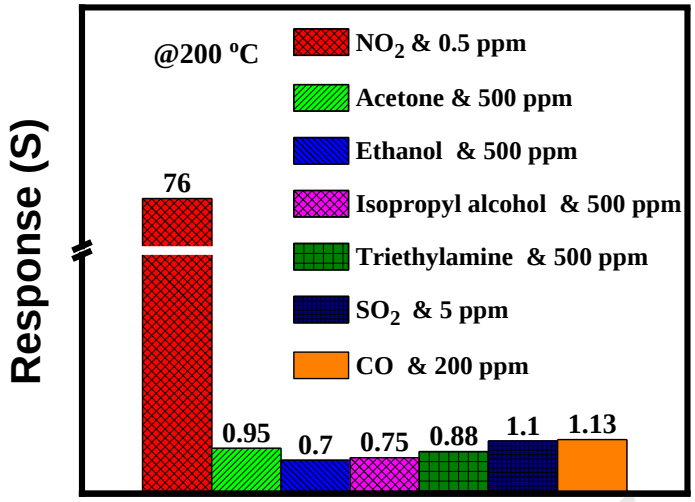

Figure 10. Selectivity of the ZnO nanoplates sensor: response values to different gases.

It is clearly that the ZnO nanoplates based sensor is suitable for application in detection of NO_2 gas in air. However, for practical application in air pollution monitoring, the effect of humidity and long–term stability is also important [20]. Thus, we tested the response to 0.5 ppm NO_2 at 200^{o}C in ambient air with different relative humidity vales of 30–90 %RH, and the data are shown in Figure 11A, and B. As shown in Figure 11A, the based resistance of the sensor decreases from 14.6 kΩ to 8.2 kΩ with an increase of relative humidity from 30% RH to 90% RH. The decrease of based resistance was ascribed to the adsorption of water molecules, which induces free electrons to the conduction band of ultra-thin porous ZnO nanoplates. In addition, the response value to 0.5 ppm NO_2 was also slightly decreased from 78 to 46 with an increase of relative humidity from 30% RH to 90% RH (Figure 11B). However, the NO_2 response of the sensor was not influenced at low relative humidity of less than 40% RH. The influence of ambient humidity on NO_2 response can be explained by the occupation of physically absorbed water on the active sites of the ZnO nanoplates, which prevent the adsorption of NO_2 molecules and results in a decrease of sensor response.

Repeatability and long–term stability of the ZnO nanoplates based sensor at 200^{o}C were also studied for the detection of 1 ppm NO_2. As shown in Figure 11C, the sensor maintained its

performance after ten consecutive cycles measurement with NO_2 gas confirming the good repeatability. After storage of 3 months in air, and a week of testing at 200^oC, the sensor still maintained its response values (Figure 11D). Such results indicate that the porous ZnO nanoplates based sensor had good repeatability and long-term stability, proving its suitability in practical applications [21].

Because NO_2 is highly toxic pollutant, thus for air quality monitoring, we tested the response of the porous ZnO nanoplates based sensor to ppb level NO_2 concentration, as shown in Figure 11E. It is clearly that the sensor could detect NO_2 gas down to ppb level with significant response values of 3.5–10 for the NO_2 concentration in the range of 5–50 ppb (Fig. 11F).

Furthermore, the response of the ZnO nanoplates based sensor to oxidation gas (SO_2), was also studied, and the data are shown Fig. S3 (Supplementary). It is clearly that the response of the sensor is relatively low of about 1.26–1.58 for SO_2 concentrations in the range of 1–5 ppm, confirming the high selectivity of the sensor over the contamination of SO_2 gas. Such results document the possibility of using the porous ZnO nanoplates based sensor to monitor NO_2 at ppb level for application in air pollution monitoring.

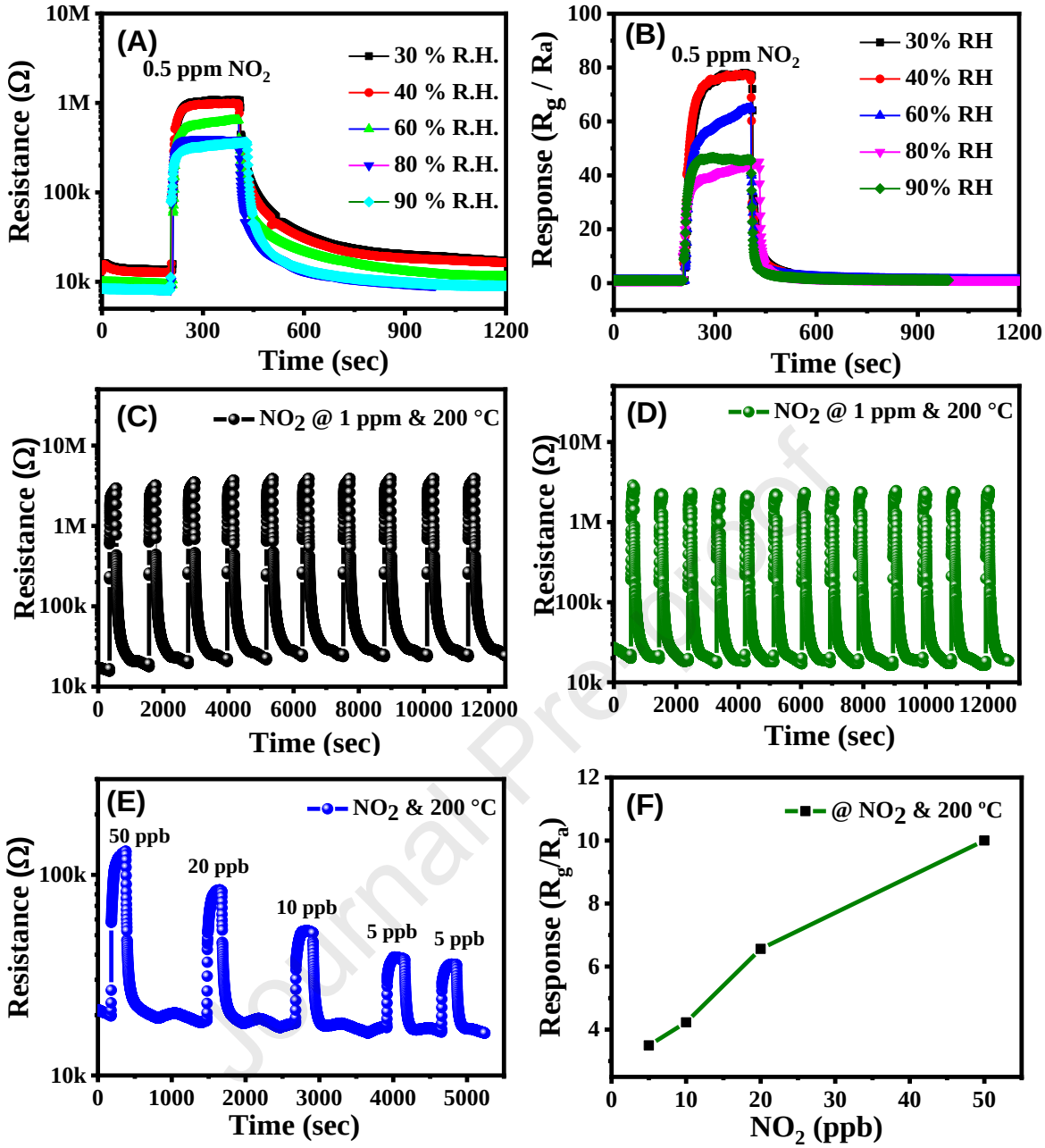

Figure 11. (A) transient resistance, and (B) response to 0.5 ppm NO_2 of the ZnO nanoplate sensor in different relative humidity values; (C) short–term, and (D) long–term stability of the sensor after storage of 3 months in air and a week of testing at 200°C; (E) transient resistance, and (F) response of the sensor to ppb level NO_2 at 200°C.

The sensing properties of metal oxide-based sensors rely on the change in electrical resistance that occurs when the gas molecules interact with the surface of the semiconductor [26,41]. Basically, when the ZnO nanoplates and nanosheets are exposed to air, oxygen is absorbed on

their surface forming oxygen anions such as O^{2-}, O^- and O_2^- and thus forming a thin depletion layer (top configuration in Fig. 12).

When NO_2 is injected into the measurement chamber, it reacts on the surface of ZnO and, being a strong oxidant, withdraws more electrons from the nanostructure, as per the following equations (bottom configuration in Fig. 11).

$$NO_{2\,(gas)} + e^- \leftrightarrow NO_2^-{}_{(ads)} \quad (1)$$

$$NO_{2\,(ads)} + O_2^-{}_{(ads)} + 2e^- \leftrightarrow NO_2^-{}_{(ads)} + 2O^-{}_{(ads)} \quad (2)$$

Although the effect is one and acts on the interface between the gas and the semiconductor creating a zone depleted of electrons, it works in two distinct ways. Along the path of the current, the depletion zones are found at the edges between different crystalline nanostructures, and create potential barriers that the electrons must overcome. When NO_2 reacts on the surface of the ZnO nanostructures withdrawing electrons, these barriers rise and the current decreases, as fewer electrons are able to pass them.

Perpendicularly to the current flow, the absorption of electrons does not create potential barriers, but only a large depletion layer. The reaction of NO_2 on the surface of the ZnO increases the thickness of this depleted area (bottom case in Fig. 12), reducing the number of electrons available for conduction. Both of these mechanisms work in the same direction: a higher concentration of NO_2 increases the thickness of the depletion layers, raising the potential barriers and decreasing the number of electrons available, and therefore increasing the resistance of the sensor.

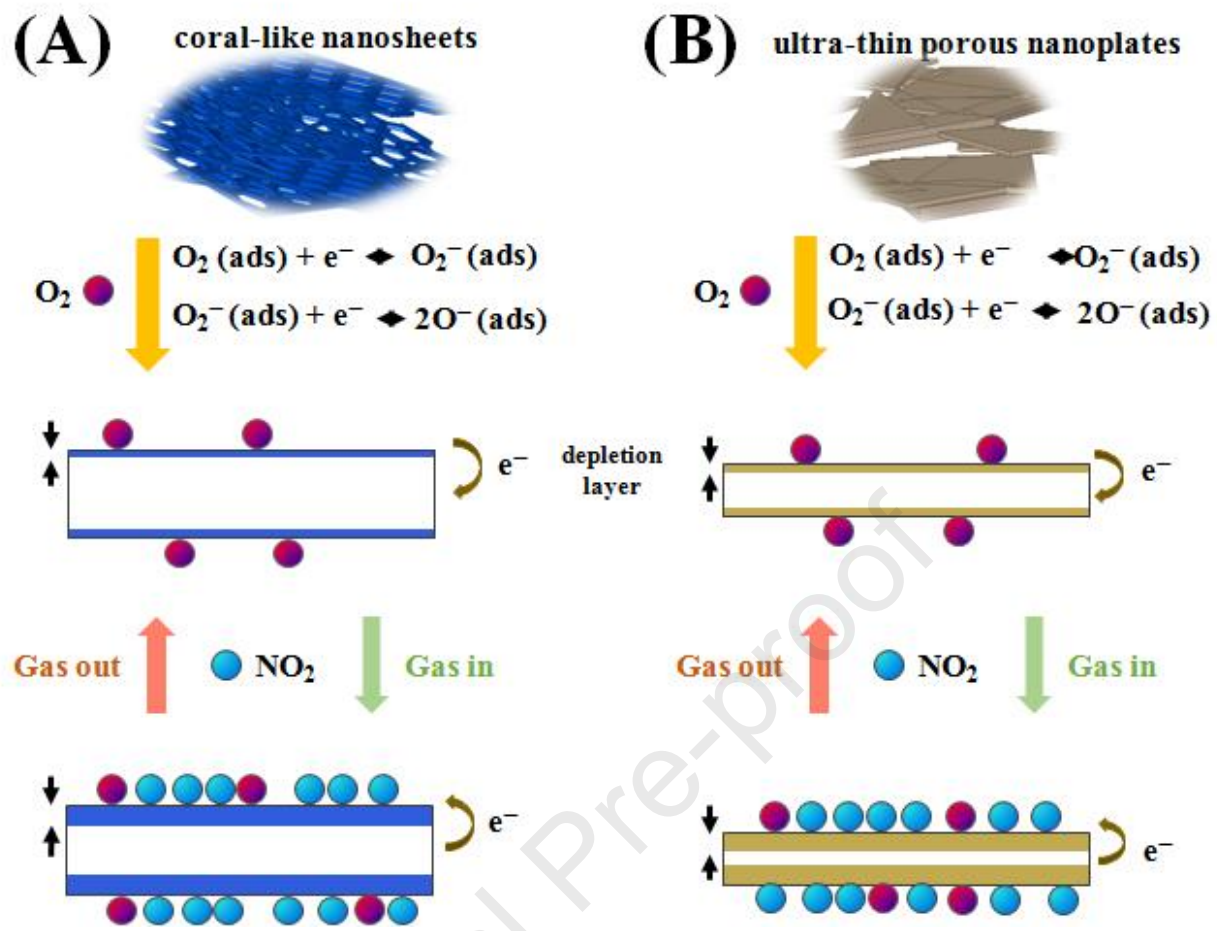

Figure 12. Schematic diagram of the NO_2 gas-sensing mechanism of the ZnO coral-like nanosheets (A) and ultra-thin nanoplates (B).

Since the width of the nanosheets and nanoplates are comparable, the higher response of the ultra-thin nanoplates is attributed to two other factors: the larger surface area [28,32] and the thinner thickness [33,34]. As seen in Fig. 12, the depth of the depletion layer is the same in the two nanostructures (indicated between the two black arrows in each case), but since the nanoplates are thinner, the relative depletion is much larger. Considering that the sensor response is the ratio between its resistance in the two conditions, it is explained why it is much higher for the ultra-thin nanoplates. The comparison between figures 6B and 7B also confirms this mechanism: the nanoplates are so thin that even very low concentrations of NO_2 heavily deplete the nanostructure, approaching response saturation.

4. Conclusion

Morphology and thickness of ZnO nanostructures were optimized for NO_2 detection by changing only the precursor salt in a simple one-step hydrothermal process. The sensing performance of coral-like nanosheets and ultra-thin nanoplates were compared. Thanks to their large surface and above all to their very thin thickness (15 nm), the ultra-thin nanoplates show sensing characteristics superior to those of coral-like nanosheets, with an excellent response of 76 to 0.5 ppm of NO_2 at 200°C. The sensor also shows very low detection limit (3 ppt) and excellent selectivity (>760) towards acetone, ethanol, isopropyl alcohol, triethylamine, SO_2 and CO, showing promise for practical applications in environmental monitoring.

Acknowledgment

This research is funded by the Hanoi University of Science and Technology (HUST) under project number T2020-SAHEP-027

Conflicts of Interest

The authors declare that they have no conflicts of interest.

References

[1] M.K. Sohal, A. Mahajan, S. Gasso, R.K. Bedi, R.C. Singh, A.K. Debnath, D.K. Aswal, Ultrasensitive yttrium modified tin oxide thin film based sub-ppb level NO2 detector, Sensors Actuators B Chem. 329 (2021) 129169. doi:10.1016/j.snb.2020.129169.

[2] E.A. Nunes Simonetti, T. Cardoso de Oliveira, Á. Enrico do Carmo Machado, A.A. Coutinho Silva, A. Silva dos Santos, L. de Simone Cividanes, TiO2 as a gas sensor: the novel carbon structures and noble metals as new elements for enhancing sensitivity – A

Review, Ceram. Int. (2021). doi:10.1016/j.ceramint.2021.03.189.

[3] L. Zhang, J. Zhang, Y. Huang, H. Xu, X. Zhang, H. Lu, K. Xu, P.K. Chu, F. Ma, Hexagonal ZnO nanoplates/graphene composites with excellent sensing performance to NO2 at room temperature, Appl. Surf. Sci. 537 (2021) 147785. doi:10.1016/j.apsusc.2020.147785.

[4] C. Han, X. Li, Y. Liu, X. Li, C. Shao, J. Ri, J. Ma, Y. Liu, Construction of In2O3/ZnO yolk-shell nanofibers for room-temperature NO2 detection under UV illumination, J. Hazard. Mater. 403 (2021) 124093. doi:10.1016/j.jhazmat.2020.124093.

[5] R.R. Kumar, T. Murugesan, A. Dash, C.-H. Hsu, S. Gupta, A. Manikandan, A. kumar Anbalagan, C.-H. Lee, N.-H. Tai, Y.-L. Chueh, H.-N. Lin, Ultrasensitive and light-activated NO2 gas sensor based on networked MoS2/ZnO nanohybrid with adsorption/desorption kinetics study, Appl. Surf. Sci. 536 (2021) 147933. doi:10.1016/j.apsusc.2020.147933.

[6] D. Chavez, C. Gomez-Solis, A.I. Mtz-Enriquez, V. Rodriguez-Gonzalez, V. Escobar-Barrios, C.R. Garcia, J. Oliva, High sensitivity of flexible graphene composites decorated with V2O5 microbelts for NO2 detection, Mater. Res. Bull. 133 (2021) 111052. doi:10.1016/j.materresbull.2020.111052.

[7] R.R. Kumar, T. Murugesan, T.-W. Chang, H.-N. Lin, Defect controlled adsorption/desorption kinetics of ZnO nanorods for UV-activated NO2 gas sensing at room temperature, Mater. Lett. 287 (2021) 129257. doi:10.1016/j.matlet.2020.129257.

[8] C.M. Hung, D.T.T. Le, N. Van Hieu, On-chip growth of semiconductor metal oxide nanowires for gas sensors: A review, J. Sci. Adv. Mater. Devices. 2 (2017) 263–285. doi:10.1016/j.jsamd.2017.07.009.

[9] W. Wang, Y. Zhang, J. Zhang, G. Li, D. Leng, Y. Gao, J. Gao, H. Lu, X. Li, Metal–organic framework-derived Cu2O–CuO octahedrons for sensitive and selective detection of ppb-level NO2 at room temperature, Sensors Actuators B Chem. 328 (2021) 129045.

doi:10.1016/j.snb.2020.129045.

[10] C. Zhang, Y. Luo, J. Xu, M. Debliquy, Room temperature conductive type metal oxide semiconductor gas sensors for NO2 detection, Sensors Actuators A Phys. 289 (2019) 118–133. doi:10.1016/j.sna.2019.02.027.

[11] S. Nundy, T. Eom, K.-Y. Song, J.-S. Park, H.-J. Lee, Hydrothermal synthesis of mesoporous ZnO microspheres as NOX gas sensor materials — Calcination effects on microstructure and sensing performance, Ceram. Int. 46 (2020) 19354–19364. doi:10.1016/j.ceramint.2020.04.278.

[12] S.N. Birajdar, P. V. Adhyapak, Palladium-decorated vanadium pentoxide as NOx gas sensor, Ceram. Int. 46 (2020) 27381–27393. doi:10.1016/j.ceramint.2020.07.223.

[13] N. Van Hieu, N. Van Duy, P.T. Huy, N.D. Chien, Inclusion of SWCNTs in Nb/Pt co-doped TiO2 thin-film sensor for ethanol vapor detection, Phys. E Low-Dimensional Syst. Nanostructures. 40 (2008) 2950–2958. doi:10.1016/j.physe.2008.02.018.

[14] V.L. Patil, S.A. Vanalakar, P.S. Patil, J.H. Kim, Fabrication of nanostructured ZnO thin films based NO 2 gas sensor via SILAR technique, Sensors Actuators B Chem. 239 (2017) 1185–1193. doi:10.1016/j.snb.2016.08.130.

[15] Y. Kang, F. Yu, L. Zhang, W. Wang, L. Chen, Y. Li, Review of ZnO-based nanomaterials in gas sensors, Solid State Ionics. 360 (2021) 115544. doi:10.1016/j.ssi.2020.115544.

[16] X. Yue, Z. Li, S. Zhao, A new electrochemical sensor for simultaneous detection of sulfamethoxazole and trimethoprim antibiotics based on graphene and ZnO nanorods modified glassy carbon electrode, Microchem. J. 159 (2020) 105440. doi:10.1016/j.microc.2020.105440.

[17] V. Gerbreders, M. Krasovska, I. Mihailova, A. Ogurcovs, E. Sledevskis, A. Gerbreders, E. Tamanis, I. Kokina, I. Plaksenkova, ZnO nanostructure-based electrochemical biosensor for Trichinella DNA detection, Sens. Bio-Sensing Res. 23 (2019) 100276. doi:10.1016/j.sbsr.2019.100276.

[18] S. Murali, P.K. Dammala, B. Rani, R. Santhosh, C. Jadhao, N.K. Sahu, Polyol mediated synthesis of anisotropic ZnO nanomaterials and composite with rGO: Application towards hybrid supercapacitor, J. Alloys Compd. 844 (2020) 156149. doi:10.1016/j.jallcom.2020.156149.

[19] P. Dammala, J. Machado, B. Rani, S. Murali, S. Devi, M. Niraj Luwang, N.K. Sahu, Synthesis of biphasic nanomaterials based on ZnO and SnO2: Application towards photocatalytic degradation of acid red dye, Nano-Structures & Nano-Objects. 18 (2019) 100292. doi:10.1016/j.nanoso.2019.100292.

[20] Y. Wang, Y. Zhou, H. Ren, Y. Wang, X. Zhu, Y. Guo, X. Li, Room-Temperature and Humidity-Resistant Trace Nitrogen Dioxide Sensing of Few-Layer Black Phosphorus Nanosheet by Incorporating Zinc Oxide Nanowire, Anal. Chem. 92 (2020) 11007–11017. doi:10.1021/acs.analchem.9b05623.

[21] Y. Zhou, Y. Wang, Y. Wang, X. Li, Y. Guo, The impact of carrier gas on room-temperature trace nitrogen dioxide sensing of ZnO nanowire-integrated film under UV illumination, Ceram. Int. 46 (2020) 16056–16061. doi:10.1016/j.ceramint.2020.03.156.

[22] P.P. Ortega, C.C. Silva, M.A. Ramirez, G. Biasotto, C.R. Foschini, A.Z. Simões, Multifunctional environmental applications of ZnO nanostructures synthesized by the microwave-assisted hydrothermal technique, Appl. Surf. Sci. 542 (2021) 148723. doi:10.1016/j.apsusc.2020.148723.

[23] N. Huang, Y. Cheng, H. Li, L. Zhao, Z. He, C. Zhao, F. Liu, L. Ding, Selective-detection NO at room temperature on porous ZnO nanostructure by solid-state synthesis method, J. Colloid Interface Sci. 556 (2019) 640–649. doi:10.1016/j.jcis.2019.07.013.

[24] S. Öztürk, N. Kılınç, Z.Z. Öztürk, Fabrication of ZnO nanorods for NO2 sensor applications: Effect of dimensions and electrode position, J. Alloys Compd. 581 (2013) 196–201. doi:10.1016/j.jallcom.2013.07.063.

[25] H. Wang, M. Dai, Y. Li, J. Bai, Y. Liu, Y. Li, C. Wang, F. Liu, G. Lu, The influence of

different ZnO nanostructures on NO2 sensing performance, Sensors Actuators B Chem. (2020) 129145. doi:10.1016/j.snb.2020.129145.

[26] T.V.A. Kusumam, V.S. Siril, K.N. Madhusoodanan, M. Prashantkumar, Y.T. Ravikiran, N.K. Renuka, NO2 gas sensing performance of zinc oxide nanostructures synthesized by surfactant assisted Low temperature hydrothermal technique, Sensors Actuators A Phys. 318 (2021) 112389. doi:10.1016/j.sna.2020.112389.

[27] L. Van Duy, N. Van Duy, C.M. Hung, N.D. Hoa, N.Q. Dich, Urea mediated synthesis and acetone-sensing properties of ultrathin porous ZnO nanoplates, Mater. Today Commun. 25 (2020) 101445. doi:10.1016/j.mtcomm.2020.101445.

[28] L. Van Duy, N.H. Hanh, D.N. Son, P.T. Hung, C.M. Hung, N. Van Duy, N.D. Hoa, N. Van Hieu, Facile Hydrothermal Synthesis of Two-Dimensional Porous ZnO Nanosheets for Highly Sensitive Ethanol Sensor, J. Nanomater. 2019 (2019) 1–7. doi:10.1155/2019/4867909.

[29] L.V. Thong, L.T.N. Loan, N. Van Hieu, Comparative study of gas sensor performance of SnO2 nanowires and their hierarchical nanostructures, Sensors Actuators B Chem. 150 (2010) 112–119. doi:10.1016/j.snb.2010.07.033.

[30] N.T. Thang, L.T. Hong, N.H. Thoan, C.M. Hung, N. Van Duy, N. Van Hieu, N.D. Hoa, Controlled synthesis of ultrathin MoS 2 nanoflowers for highly enhanced NO 2 sensing at room temperature, RSC Adv. 10 (2020) 12759–12771. doi:10.1039/D0RA00121J.

[31] S. Agarwal, P. Rai, E.N. Gatell, E. Llobet, F. Güell, M. Kumar, K. Awasthi, Gas sensing properties of ZnO nanostructures (flowers/rods) synthesized by hydrothermal method, Sensors Actuators B Chem. 292 (2019) 24–31. doi:10.1016/j.snb.2019.04.083.

[32] C.M. Hung, N.D. Hoa, N. Van Duy, N. Van Toan, D.T.T. Le, N. Van Hieu, Synthesis and gas-sensing characteristics of α-Fe2O3 hollow balls, J. Sci. Adv. Mater. Devices. 1 (2016) 45–50. doi:10.1016/j.jsamd.2016.03.003.

[33] H.M. Tan, C. Manh Hung, T.M. Ngoc, H. Nguyen, N. Duc Hoa, N. Van Duy, N. Van

Hieu, Novel Self-Heated Gas Sensors Using on-Chip Networked Nanowires with Ultralow Power Consumption, ACS Appl. Mater. Interfaces. 9 (2017) 6153–6162. doi:10.1021/acsami.6b14516.

[34] P.-S. Cho, K.-W. Kim, J.-H. Lee, NO2 sensing characteristics of ZnO nanorods prepared by hydrothermal method, J. Electroceramics. 17 (2006) 975–978. doi:10.1007/s10832-006-8146-7.

[35] F.-T. Liu, S.-F. Gao, S.-K. Pei, S.-C. Tseng, C.-H.J. Liu, ZnO nanorod gas sensor for NO2 detection, J. Taiwan Inst. Chem. Eng. 40 (2009) 528–532. doi:10.1016/j.jtice.2009.03.008.

[36] J.X. Wang, X.W. Sun, Y. Yang, C.M.L. Wu, N–P transition sensing behaviors of ZnO nanotubes exposed to NO 2 gas, Nanotechnology. 20 (2009) 465501. doi:10.1088/0957-4484/20/46/465501.

[37] R.K. Sonker, S.R. Sabhajeet, S. Singh, B.C. Yadav, Synthesis of ZnO nanopetals and its application as NO2 gas sensor, Mater. Lett. 152 (2015) 189–191. doi:10.1016/j.matlet.2015.03.112.

[38] X. Chen, Y. Shen, W. Zhang, J. Zhang, D. Wei, R. Lu, L. Zhu, H. Li, Y. Shen, In-situ growth of ZnO nanowire arrays on the sensing electrode via a facile hydrothermal route for high-performance NO2 sensor, Appl. Surf. Sci. 435 (2018) 1096–1104. doi:10.1016/j.apsusc.2017.11.222.

[39] K. Shingange, H.C. Swart, G.H. Mhlongo, Au functionalized ZnO rose-like hierarchical structures and their enhanced NO 2 sensing performance, Phys. B Condens. Matter. 535 (2018) 216–220. doi:10.1016/j.physb.2017.07.039.

[40] H. Wang, M. Dai, Y. Li, J. Bai, Y. Liu, Y. Li, C. Wang, F. Liu, G. Lu, The influence of different ZnO nanostructures on NO2 sensing performance, Sensors Actuators B Chem. 329 (2021) 129145. doi:10.1016/j.snb.2020.129145.

[41] C. Zhang, G. Liu, X. Geng, K. Wu, M. Debliquy, Metal oxide semiconductors with highly concentrated oxygen vacancies for gas sensing materials: A review, Sensors Actuators A

Phys. 309 (2020) 112026. doi:10.1016/j.sna.2020.112026.

Declaration of interests

☒ The authors declare that they have no known competing financial interests or personal relationships that could have appeared to influence the work reported in this paper.

☐The authors declare the following financial interests/personal relationships which may be considered as potential competing interests: